NRC Publications Archive
Archives des publications du CNRC

Alternative coating technologies for metal-ceramic nanocomposite films : potential application for solar thermal absorber

Bensebaa, F.; Di Domenicantonio, D.; Scoles, L.; Kingston, D.; Mercier, P.; Marshall, G.

This publication could be one of several versions: author's original, accepted manuscript or the publisher's version. / La version de cette publication peut être l'une des suivantes : la version prépublication de l'auteur, la version acceptée du manuscrit ou la version de l'éditeur.
For the publisher's version, please access the DOI link below./ Pour consulter la version de l'éditeur, utilisez le lien DOI ci-dessous.

Publisher's version / Version de l'éditeur:
https://doi.org/10.1093/ijlct/ctt081
International Journal of Low-Carbon Technologies, 2014, 0, pp. 1-5, 2014-03-26

NRC Publications Record / Notice d'Archives des publications de CNRC:
https://nrc-publications.canada.ca/eng/view/object/?id=32363412-b44a-4f29-b368-f5f0915a91c7
https://publications-cnrc.canada.ca/fra/voir/objet/?id=32363412-b44a-4f29-b368-f5f0915a91c7

Access and use of this website and the material on it are subject to the Terms and Conditions set forth at
https://nrc-publications.canada.ca/eng/copyright
READ THESE TERMS AND CONDITIONS CAREFULLY BEFORE USING THIS WEBSITE.

L'accès à ce site Web et l'utilisation de son contenu sont assujettis aux conditions présentées dans le site
https://publications-cnrc.canada.ca/fra/droits
LISEZ CES CONDITIONS ATTENTIVEMENT AVANT D'UTILISER CE SITE WEB.

Questions? Contact the NRC Publications Archive team at PublicationsArchive-ArchivesPublications@nrc-cnrc.gc.ca. If you wish to email the authors directly, please see the first page of the publication for their contact information.

Vous avez des questions? Nous pouvons vous aider. Pour communiquer directement avec un auteur, consultez la première page de la revue dans laquelle son article a été publié afin de trouver ses coordonnées. Si vous n'arrivez pas à les repérer, communiquez avec nous à PublicationsArchive-ArchivesPublications@nrc-cnrc.gc.ca.

National Research Council Canada
Conseil national de recherches Canada
Canada

International Journal of Low-Carbon Technologies Advance Access published March 26, 2014

Alternative coating technologies for metal–ceramic nanocomposite films: potential application for solar thermal absorber

F. Bensebaa*, D. Di Domenicantonio, L. Scoles, D. Kingston, P. Mercier and G. Marshall

Energy, Mining and Environment, National Research Council of Canada, 1200 Montreal Rd, Ottawa, ON, Canada K1A 0R6

Abstract

Metal–ceramic nanocomposite films for solar absorbers have been obtained by electro-deposition. This coating technique uses a mixed solution of nickel nanoparticles and sub-micron alumina particles. The relative ratio of Ni-to-Al in these films is varied by tuning the concentration of nickel and alumina particles in the starting solution. Three films with different Ni/Al ratio have been prepared and characterized with X-ray photo-electron spectroscopy and scanning electron microscope. Even in absence of any heat treatment, significant amount of nickel in metallic state has been found in all three samples.

Keywords: electrodeposition; nanoparticle; coating; metal; solar

*Corresponding author:
farid.bensebaa@nrc.ca

Received 25 July 2013; revised 27 September 2013; accepted 26 October 2013

1 INTRODUCTION

Nanostructured metallic nickel films are used for solar heat absorption [1], electromagnetic interference (EMI) shielding [2], tribology [3], magnetic [4], photo-catalytic [5], energy storage [6] and automotive lightweight metal matrix composites (MMC) [7] applications. These films are obtained by sputtering [8], chemical vapour deposition (CVD) [9], electroless deposition [10] and electro-deposition [6, 11] processes. Other techniques have been also used to form metallic, alloyed and composite films containing bulk or nanostructured nickel structures. Cost-effective deposition techniques are required for a wider acceptance of these nanostructured nickel films.

Besides optimizing the use of raw materials, nickel nanocomposite films provide performance attributes when compared with uniform bulk nickel coating. Increased active interface between the different battery layers may give rise to higher specific current density and faster charging/discharging rates [6]. There are numerous examples where nanostructured nickel enhances catalytic, magnetic, thermo-optical and tribological properties. Integration of nanocrystalline metallic nickel in a non-conductive matrix improves mechanical, chemical and thermal stability. Nickel-based precipitates increase the mechano-chemical properties of coatings and base materials.

Nickel nanoparticles imbedded in oxide matrix provide high solar absorption with low emissivity [1, 8] and improved stability at high temperature even under aggressive chemical environments. Ni/Al_2O_3 nanocomposite coating has a low emittance and high absorption coefficient even at high operating temperatures [12, 13]. Controlling the size of nickel nanoparticles and their distribution within the dielectric matrix is critical to achieve higher absorption to emissivity ratio. Thus, the selected deposition technique should allow the possibility of controlling size and distribution along the surface normal. Furthermore, the deposition technique should allow cost effective large-area film-coating.

Solar absorber consisting of a metallic substrate coated with a high solar absorption coefficient film is a critical component of the solar thermal system. Several techniques are used to produce these coating films. Starting from the raw materials, a nanopowder formulation is produced to suite the film characteristics and the coating technique requirements. Once optimized and tested, the coated substrate is packaged and integrated within the overall solar thermal system. The overall value chain consisting of the five main extraction, manufacturing and installations steps is summarized in Scheme 1. In this article, we will focus mainly in the third step (coating film formation), although Step 2 (formulation) and Step 4 (optimization and testing) will be also discussed briefly.

Downloaded from http://ijlct.oxfordjournals.org/ at Canada Institute for STI on March 27, 2014

International Journal of Low-Carbon Technologies 2014, 0, 1–5
© Crown copyright 2014.
doi:10.1093/ijlct/ctt081

Electro-deposition often referred as electrophoretic [14] and electroplating [11, 15] have been used in the past to produce graded Ni-Al_2O_3 films. In the case of electrophoretic deposition (EPD), dispersed nickel and alumina particles are used as precursors. Ionic nickel and aluminium precursors dispersed in the solution bath are used in the case of electroplating. Both approaches have their own advantages and drawbacks. EPD techniques allow preparation of films with thickness varying from <10 nm up to several hundred micrometers [16, 17]. Specific advantages of EPD include rapidity, low deposition cost, scalability and wide composition and thickness ranges. Furthermore, there are no limitations in terms of shape and size of the substrate. EPD has been already used as an industrial process over more than 160 years [17]. Electro-deposition is cost-effective when compared with physical vapour deposition (PVD) techniques for metal-dielectric composite-coating productions [8, 18, 19].

Recently EPD has been pursued as a scalable and cost effective fabrication process for nickel-based coating films [20, 21]. EPD is a cost-effective and green process allowing quick deposition of nickel nanoparticles over large surface areas for solar absorbers. To allow higher absorption coefficient and lower emissivity, a graded nanostructure nickel/alumina coating has been pursued [13]. Two different composition layers deposited by spin coating on aluminium substrates have been obtained. The first layer is composed of an 80% nickel–20% (Ni80) alumina film followed by a 40% nickel–60% alumina (Ni40) film [13]. Although it is simple, spin coating has several limiting factors for industrial applications. For example spin-coating process leads to high materials losses, non-uniform composition and thickness and low production efficiency.

One drawback of EPD used in metal-dielectric film production is the requirement of high temperature, up to 1000°C, and longer annealing times, up to several days under hydrogen controlled atmosphere [16]. In this study, we will use metallic nickel nanoparticles as precursors for EPD. X-ray photo-electron spectroscopy (XPS) will be used to probe the oxidation state of the film obtained with different nickel concentration before any post-treatment. Additionally, the effect of the relative nickel to alumina starting composition will be investigated.

2 EXPERIMENTAL PART

Aluminium oxide (alumina) and nickel powder particles are obtained from Alfa-Aesar (Ward Hill, USA) and Vale-Inco (Toronto, Canada), respectively. The alumina sample has an average particle size of around 400 nm. The average particle size of the nickel powder is around 50 nm. Other size distributions are available although not evaluated in this study. These relatively small metallic nickel nanoparticles are obtained by high-temperature carbonyl method following an optimization of the fabrication process [22]. EPD is carried out in a two electrodes cell with a magnesium working electrode and a gold counter electrode. Appropriate amounts of nickel and alumina powders are first mixed with 50 ml ethanol solvent and sonicated overnight. Longer sonication is required to obtain higher quality films. Once dispersed, these two solutions are mixed in different proportions to form the electrolytic to obtain a targeted coating composition (Figure 1). The pH of the mixed electrolytic solution is adjusted to around 4.6 by HCl (acidic side) and NH_4OH (basic side). The deposition is conducted under a constant stirring using 10 V applied voltage for at least 5 min duration. Three coating samples were obtained by varying the Ni:Al ratio in the starting solution. A nominal weight composition of 78, 46 and 22% nickel is initially targeted for the final film (Figure 1). These films are referred by Ni_{22}, Ni_{46} and Ni_{78} symbols, respectively.

The samples were then examined using a JEOL 840A scanning electron microscope equipped with an Oxford Instruments 6560 INCAx-sight light element energy-dispersive X-ray (EDX) spectrometer. The spectrometer consists of a super atmospheric thin window and Si(Li) crystal that can detect Be to U and has a spectral resolution of 129 eV. All photos and analyses were taken using an accelerating voltage of 20 kV and a working distance of 15 mm. A total live count time of 60 s was used for each analysis.

XPS data were obtained using a Kratos Axis Ultra XPS equipped with a monochromated Al X-ray source (X-ray photon characteristic energy, $h_v = 1486.6$ eV). Analyses were carried out using an accelerating voltage of 14 kV and a current of 10 mA. Chamber pressure during analysis was typically in the

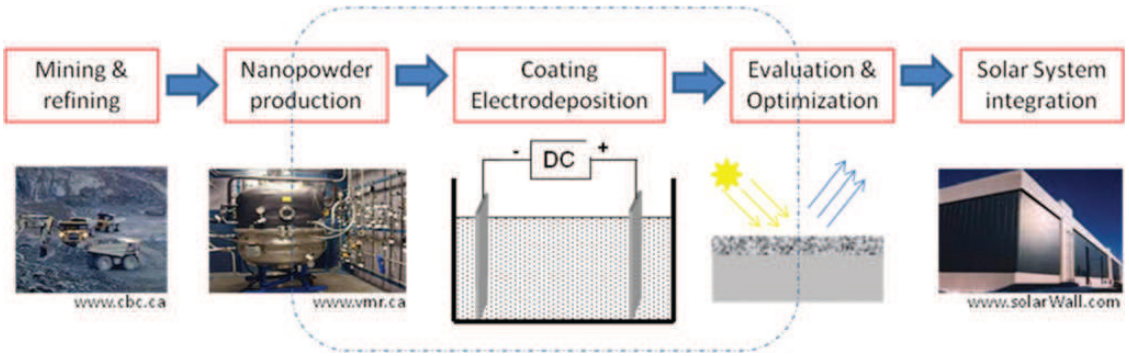

Scheme 1. *Overall value-chain of the solar thermal system for solar heat production. Dashed rectangle indicates parts of the value-chain covered in this manuscript.*

Downloaded from http://ijlct.oxfordjournals.org/ at Canada Institute for STI on March 27, 2014

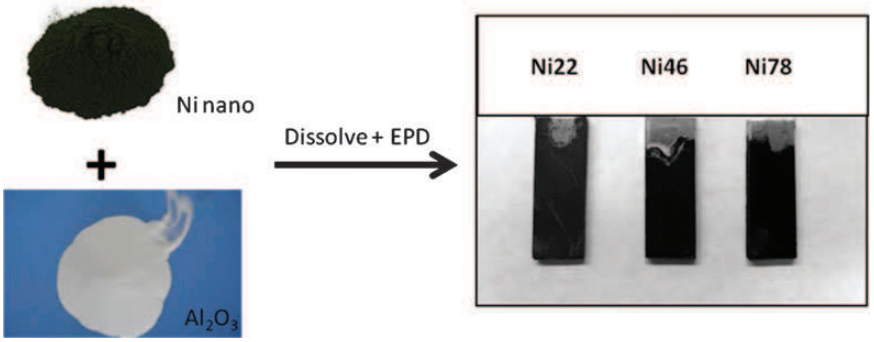

Figure 1. *Simplified two-steps process for the production of nickel-alumina nanocomposite films. Ni22, Ni48 and Ni78 correspond to nominal nickel weight compositions of 22, 46 and 78%, respectively.*

order of 2.67×10^{-10} Pa. Sample charge build-up was compensated by using the Axis charge balancing system. Binding energy values were referenced to the main carbon peak set to 285.0 eV.

3 RESULTS

Photo-correlation spectroscopy revealed that the average size of the starting nickel powder is around 50 nm [23], consistent with SEM data. Brunauer–Emmett–Teller (BET) measurements showed that the average size distribution is about 60 nm. In the case of commercially available alumina particles, the datasheet indicates an average size of 400 nm.

Besides the size distribution of the starting powders, there are numerous experimental parameters that could affect the overall film quality. Preliminary testing showed that pH and relative nanoparticle concentrations are critical. Other important parameters include applied voltage, deposition time, viscosity and substrate type and pre-treatment. Films with three different relative concentrations are obtained. Uniform and relatively dense black film has been obtained within 5 min of deposition.

Backscattered SEM pictures of typical areas from the $Ni_{22}Al_{78}$, $Ni_{46}Al_{54}$ and $Ni_{78}Al_{22}$ samples are shown in Figure 2. In the case of the $Ni_{22}Al_{78}$ and $Ni_{46}Al_{54}$ samples, crack-free coating with an apparent variation in film thickness is observed. The third sample ($Ni_{78}Al_{22}$) showed a more uniform film thickness although an evidence for cracks is noticed throughout the film surface. EDXA of the $Ni_{22}Al_{78}$ and $Ni_{46}Al_{54}$ samples showed the presence of two different areas. One area (the majority of the surface) containing a coating film with a composition consistent with the starting Al/Ni composition ratio. The second area consists of brighter spots where excess of Ni is observed. The brighter spots shown in Figure 2a and b are not observed in Figure 2c related to $Ni_{78}Al_{22}$.

The Ni/Al ratio is estimated by averaging the atomic concentration obtained from around 20 spots. Values of 0.17, 0.32 and 1.6 have been obtained for $Ni_{22}Al_{78}$, $Ni_{46}Al_{54}$ and $Ni_{78}Al_{22}$, respectively. These experimental values are lower than the theoretical ratio (0.28, 0.85 and 3.5, respectively) estimated from the starting elemental composition. This difference between the composition obtained with SEM and the theoretical composition is higher with low alumina concentrations. There are two possible explanations. One is the non-uniform deposition normal to the surface of the two powder materials (gradient composition). Thus, one could hypothesize that the smaller nickel nanoparticle will deposit first followed by the larger alumina particles. Indeed, the deposition kinetics of larger particles (alumina) is expected to be relatively slower. Furthermore, it is possible that smaller particles will aggregate to form larger particles. Another explanation, more plausible, is related to the fact that alumina particles sediment much faster than nickel particles. Indeed, alumina particles are more difficult to disperse in the ethanol solution. In both cases, the preferential deposition is a valuable technology advantage in the quest for functional graded materials with top alumina layer. In particular, starting particle surface compositions could be used to control the deposition kinetics.

XPS analysis also revealed the presence of Al and Ni in all three samples. It is consistent with XPS data reported elsewhere [24]. The estimated relative nickel content is about 9, 31 and 62% for the $Ni_{22}Al_{78}$, $Ni_{46}Al_{54}$ and $Ni_{78}Al_{22}$ samples, respectively (Figure 3). Composition obtained with XPS and SEM showed similar trends. In both cases, nickel content is lower than expected. This confirms the preferential surface segregation of alumina particle. Increasing Ni:Al trend ratio is reflected by the ratio obtained by XPS and SEM in both cases. Relatively higher Al concentration is expected given the surface sensitivity of XPS.

The oxidation state of Ni and the relative ratio of Ni/NiO_x are also critical for some applications. To probe the different binding states, high-resolution XPS has been recorded from the $Ni_{22}Al_{78}$, $Ni_{46}Al_{54}$ and $Ni_{78}Al_{22}$ samples. We have used the peak fitting and quantification reported by Biesinger *et al.* [24]. As summarized in Table 1, three different nickel-based compounds are observed. Although the absolute values of the relative concentration of the different chemical states vary, the ratio of metallic nickel to the metallic oxides is relatively constant. A value of around 12 is estimated for metallic nickel to non-metallic nickel concentration ratios for all three samples. However, it is

Downloaded from http://ijlct.oxfordjournals.org/ at Canada Institute for STI on March 27, 2014

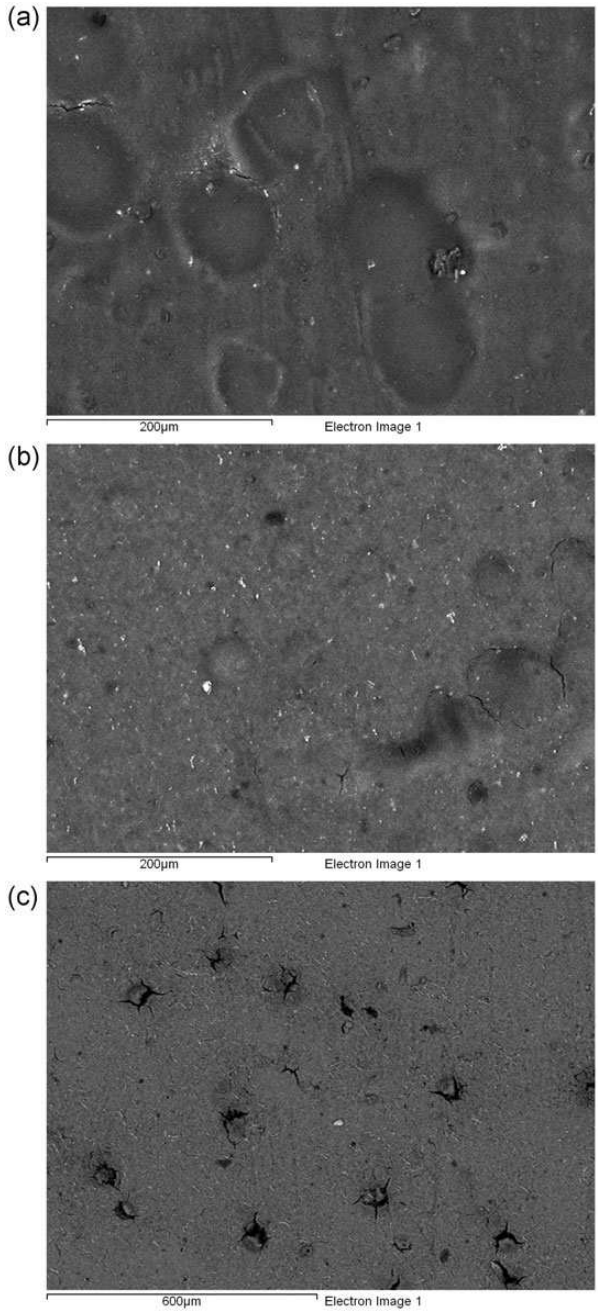

Figure 2. *Backscattered SEM images of Ni_{22} (**a**), Ni46 (**b**) and Ni78 (**c**) samples.*

worth noting that this ratio does not reflect the actual ratio of the films, given the surface sensitivity of XPS. Indeed, XPS detects only the first 10 nm, with an exponential sensitivity reduction from top to the depth of these nickel nanoparticles.

Nickel nanoparticles are expected to have a core–shell structure. The shell layer will consist of a nickel oxide structure. To estimate the thickness of the oxide, we have used the following formula [24–26]:

$$d_{ox} = \lambda_{ox} \cdot sin\theta \cdot \ln[(N_m/N_{ox}) \cdot (\lambda_m/\lambda_{ox}) \cdot (I_{ox}/I_m) + 1]$$

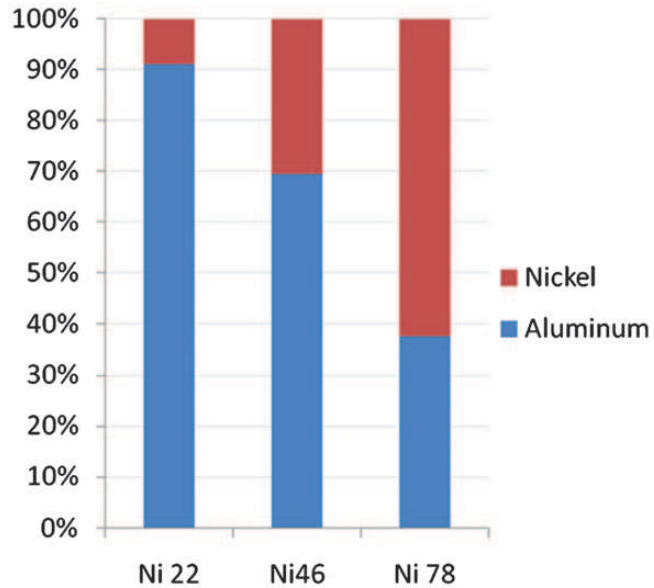

Figure 3. *Relative elemental Ni and Al contents in the three films.*

Table 1. *Relative concentration of the main nickel chemical states as probed by XPS.*

	Ni22	Ni46	Ni78
Ni	0.25	0.68	0.56
NiO	0.82	1.98	1.82
$Ni(OH)_2$	1.25	3.51	3.10
$Ni/(NiO+ Ni(OH)_2) \times 10^{-2}$	12.0	12.4	11.4

where I_m is the inelastic mean free path of the metal, I_{ox} is the inelastic mean free path of the oxide, N_m is the volume density of the metal atoms in the metal, N_{ox} is the volume density of the metal atoms in the oxide, λ_m is the inelastic mean free path of the metal, λ_{ox} is the inelastic mean free path of the metal oxide, and θ is the photo-electron take-off angle (90°).

Ni, NiO and $Ni(OH)_2$ densities are assumed to 8.90, 6.67 and 4.15 g/cm^3, respectively [24]. An inelastic mean free path of 1.798, 2.206 and 1.08 nm have been assumed for NiO, $Ni(OH)_2$ and Ni, respectively [24]. It is worth noting that this formula is established for uniform oxide on a flat metal substrate. We will assume this formula applies also for spherical core–shell-oxidized nickel nanoparticles. For the sake of calculation, we will consider an equally weighed average for both volume density and inelastic mean free path for the non-metallic nickel. In this case, we will consider average numbers of 5.41 g/cm^3 and 2.002 nm for the density and the inelastic mean free path of non-metal nickel species, respectively.

Using the formula and constant values above, the overall oxide thickness is estimated to around 4.3 nm. This is slightly higher than the oxide thickness reported on flat nickel substrate estimated to around 3.6 nm [24]. This difference is probably due

Downloaded from http://ijlct.oxfordjournals.org/ at Canada Institute for STI on March 27, 2014

to the assumption of a relatively flat film structure. However, other experimental parameters may explain this difference. A more accurate quantitative XPS analysis has been used to account for variable take-off angle of photo-electron on a spherical particle [27]. Using unweighed take-off angle of photo-electron an error of $<23\%$ has been obtained. In a more recent publication, Shard *et al.* used an XPS topofactor to estimate over-layer thickness of spherical particles [28]. Using normal collection geometry to minimize the shadowing effect, these authors used a topofactor of 0.67 in the case of spherical sample. This factor is less than the ratio $3.6/4.3 = 0.84$ of the oxide thickness estimated for the spherical particles in this work and the flat substrate reported by Biesinger *et al.* [24].

We are currently evaluating the effect of concentration on the thermo-optical properties of theses nanostructured films. Preliminary data showed that the optical reflectance of non-annealed samples increases with nickel content within the film. This may indicate that solar absorption coefficient increases with relative concentration of nickel nanoparticles. Multilayer structure with variable nickel concentration is achievable with EPD, which could allow reduced emissivity coefficient. More investigations are underway to understand and optimize the thermo-optical properties of these films.

4 CONCLUSIONS

Three films with a nominal starting composition of $Ni_{22}Al_{78}$, $Ni_{46}Al_{54}$ and $Ni_{78}Al_{22}$ are obtained by electrophoretic deposition under room temperature conditions. The film with the highest nickel content is uniform, although it gives rise to some type of surface film discontinuity. It is possible to fabricate variable metallic nickel-based nanocomposite films without subjecting the materials to longer annealing time at high temperature under hydrogen atmosphere. However, it is likely that the annealing may contribute to improved properties.

ACKNOWLEDGEMENTS

The authors express their gratitude to Steve Baksa (Vale-Inco, Canada) for providing nickel nanopowder used in this study. Contribution from Prof. Jose Etcheverry is appreciated.

REFERENCES

[1] Sathiaraj TS, Thangaraj R, Agnihotri OP. High absorptance and low emittance m-coated Ni-Al,O, solar absorbers. *J Phys D Appl Phys* 1990;**23**: 250–4.

[2] Liu Q, Zhang A, Fan T, *et al*. Amorphous carbon-matrix composites with interconnected carbon nano-ribbon networks for electromagnetic interference shielding. *Carbon* 2008;**46**:461–5.

[3] Sahoo P, Kalyan Das S. Tribology of electroless nickel coatings—a review. *Mater Des* 2011;**32**:1760–75.

[4] Jung A, Natter H, Hempelmann R, *et al*. Study of the magnetic flux density distribution of nickel coated aluminum foams. *J Phys Conf Ser* 2010;**200**:082011–14.

[5] Yoshinaga M, Yamamoto K, Sato N, *et al*. Remarkably enhanced photocatalytic activity by nickel nanoparticle deposition on sulfur-doped titanium dioxide thin film. *Appl Catal B Environ* 2009;**87**:239–44.

[6] Zhang H, Yu X, Braun PV. Three-dimensional bicontinuous ultrafast-charge and -discharge bulk battery electrodes. *Nat Nanotechnol* 2011;**6**: 277–81.

[7] Farooqa M, Rajab I. Optimisation of metal sputtered and electroplated substrates for solar selective coatings. *Renew Energy* 2008;**33**:1275–85.

[8] Presting H, König U. Future nanotechnology developments for automotive applications. *Mater Sci Eng C* 2003;**23**:737–41.

[9] Bakovets V, Mitkin V, Gelfond NV. Mechanism of Ni film CVD with a $Ni(Ktfaa)_2$ precursor on a silicon substrate. *Chem Vap Depos* 2005;**11**:368–74.

[10] Agarwala RC, Ararwala V. Electroless alloy/composite coatings: a review. *Sadhana* 2003;**28**:475–93.

[11] Barmak K, Banvic SW, Petronis CM, *et al*. Structure of electrodeposited graded composite coatings of Ni-Al-Al_2O_3. *J Microsc* 1997;**185**:265–74.

[12] Kennedy CE. Review of mid- to high-temperature solar selective absorber materials. National Renewable Energy Laboratory (NREL) report, 2002.

[13] Boström T, Jensen J, Valizadeh S, *et al*. ERDA of Ni–Al_2O_3/SiO_2 solar thermal selective absorbers. *Sol Energy Mater Sol Cells* 2004;**92**:1177–82.

[14] Nagarajan N, Nicholson PS. Nickel-alumina functionally graded materials by electrophoretic deposition. *J Am Ceram Soc* 2004;**87**:2053–7.

[15] Bahrololoom ME, Sani R. The influence of pulse plating parameters on the hardness and wear resistance of nickel–alumina composite coatings. *Surf Coat Technol* 2005;**192**:154–63.

[16] Besra L, Liu M. A review on fundamentals and applications of electrophoretic deposition (EPD). *Prog Mater Sci* 2007;**52**:1–61.

[17] Van Tassel T, Randall CA. Mechanisms of electrophoretic deposition. *J Mater Sci* 2004;**39**:867–79.

[18] Navinsek B, Panjan P, Milosev I. PVD coatings as an environmentally clean alternative to electroplating and electroless processes. *Surf Coat Technol* 1999;**116–119**:476–87.

[19] Wackelgard E, Hultmark G. Industrially sputtered solar absorber surface. *Sol Energy Mater Solar Cells* 1999;**54**:165–70.

[20] Luo K, Shi N, Cong H, *et al*. Electrophoretic deposition of nickel, iron and aluminum nanoparticles on carbon fibers. *Carbon* 2008;**46**:461–5.

[21] Yang X, Peng X, Wang F. Hot corrosion of a novel electrodeposited Ni–6Cr–7Al nanocomposite under molten (0.9Na, 0.1 K)$_2SO_4$ at 900°C. *Scripta Mater* 2007;**56**:891–4.

[22] Bensebaa F, L'Ecuyer P, Pleizier G, *et al*. Characterization of nickel nanoparticles. NRC Client Report, July 2002.

[23] Baksa S. Vale-INCO, Private communications, March 2010.

[24] Biesinger MC, Payne BP, Lau LWM, *et al*. Smart RSC. X-ray photoelectron spectroscopic chemical state quantification of mixed nickel metal, oxide and hydroxide systems. *Surf Interface Anal* 2009;**41**:324–32.

[25] Strohmeier BR. An ESCA method for determining the oxide thickness on aluminum alloys. *Surf Interface Anal* 1990;**15**:51–6.

[26] Carlson TA, McGuire GE. Study of the X-ray photoelectron spectrum of tungsten-tungesten oxide as a function of thickness of the surface oxide layer. *J Electron Spectrosc Relat Phenom* 1972/1973;**1**:161–8.

[27] Frydman A, Castner DG, Schmal M, *et al*. A method for accurate quantitative XPS analysis of multimetallic or multiphase catalysts on support particles. *J Catal* 1995;**157**:133–44.

[28] Shard AG, Wang J, Spencer SJ. XPS topofactors: determining overlayer thickness on particles and fibres. *Surf Interface Anal* 2009;**41**:541–8.

[29] Landolt D. Electrodeposition science and technology in the last quarter of the twentieth century. *J Electrochem Soc* 2002;**149**:S9–S20.

Downloaded from http://ijlct.oxfordjournals.org/ at Canada Institute for STI on March 27, 2014